Special Issue on "Theoretical and Computational Chemistry"

J. Indian Chem. Soc.,
Vol. 96, July 2019, pp. 883-893

H_2O dissociation on step Ni(211) surface: Mode selectivity under vibrational adiabaticity

Sudipta Roy, Nayanthara K. J. and Ashwani K. Tiwari*

Department of Chemical Sciences, Indian Institute of Science Education and Research Kolkata, Mohanpur- 741 246, West Bengal, India

E-mail: ashwani@iiserkol.ac.in

Manuscript received online 19 April 2019, revised and accepted 20 May 2019

Dissociation of water molecule on metal surface has been receiving extensive attention due to its industrial importance. Water adsorption and dissociation on step Ni(211) surface is studied from first-principle calculations and slab model. Effect of surface temperature and molecule-phonon coupling is investigated by including lattice motion calculation using sudden model and it has been found that increasing temperature of metal surface results in enhancement of catalytic activity of the surface toward water dissociation. Dynamics study of this reaction is investigated using Reaction Path Hamiltonian method. 1-D PES is constructed by taking into account all 9 molecular degrees of freedom. Normal mode calculation of all the molecular geometries of water molecule along the whole reaction path is calculated and it shows that symmetric and bending mode exhibit significant mode softening near the transition state, asymmetric mode does not exhibit any change of frequency along the whole reaction path. Under adiabatic approximation order of reaction probability for different vibrational normal modes is symmetric > bending > asymmetric > ground state.

Keywords: Water dissociation, heterogeneous catalysts, step surfaces, mode selectivity.

1. Introduction

The interaction of water with transition metal surfaces have been a subject of immense significance in the recent time. The amount of research carried out in the water adsorption and dissociation by both experimentalists and theoreticians have seen an augmentation owing to its industrial applications namely steam reforming of alcohol and methane, water gas shift reaction and electrochemistry[1–4]. Methane and water react over a catalyst in the steam reforming of methane to form H_2 + CO. In the water gas shift reaction ($CO + H_2O = CO_2 + H_2$), CO formed from the steam reforming of methane react with a second water molecule to form H_2. This water gas shift reaction is one of the premier catalytic processes for the generation of hydrogen. Water gas shift reaction carried out in low temperatures, H_2O dissociation is found to be rate determining step using metal based catalysts[5–8]. Cu based metals are used as catalyst for water gas shift reaction in industrial process, but it has been observed that Ni is more reactive towards water gas shift reaction than Cu[9].

It is encouraged to possess an atomic level knowledge about how water molecules interact with metal surfaces to understand the catalytic mechanistic pathways. Even though numerous theoretical calculations have been carried out for water dissociation on metal surfaces, most of them are density functional theory (DFT) calculations[10–13]. The study of dynamics of direct dissociative chemisorption of H_2O started only recently[14–20]. In this dissociation reaction H_2O breaks one of its O-H bonds as it undergoes collision with metal surface and thus formed H and OH fragments and get chemisorbed to the metal surface. It has also come into notice from experiments that in unimolecular and bimolecular gas phase reactions an increase in reactivity is observed by the vibrational excitation of reagents[21,22]. This could be attributed to both mode selectivity as well as bond selectivity. Mode selectivity is determined by the excitation of a particular vibrational mode, that result the product formation and not just its energy and bond selectivity is by selective vibrational excitation that results preferential cleavage of a particular bond[23,24]. There is quite a lot of research in connection with bond and mode selectivity has already been done on methane on metal surfaces[25–28]. The initial quantum dynamical

studies on H_2O dissociation was first carried out on Cu(111) surface[14,29,30]. The first molecular beam experiment on the water dissociation on Ni(111) had been carried out recently[31]. It was also shown that D_2O, HOD on Ni(111) surface exhibited mode selectivity[32]. Majority of these calculations are done on (111), (100) metal surfaces[33,34]. These surfaces are smooth and hence it doesn't give a real picture of actual catalysts which are believed to be rough on an atomistic view. Such a scenario and experimental evidences reveal that reactions at defect sites such as steps proceed fast[35,36].

Dynamics study of H_2O dissociation have been performed extensively in recent time using a quasi-classical trajectory method[16] or wave packet propagation method[29,37–40] on a high dimensional potential energy surfaces. The problem with quasi classical trajectory method is that it does not take account for the tunneling process, which plays a major role for water dissociation on solid surfaces. Therefore quantum dynamics study is inevitable for the dynamics study[14,41]. The accurate 9-D PES gives reasonably good results for dissociative chemisorption of water on metal surfaces. But the computational effort as well as expense is really huge[16,29] as a large number of *ab initio* data points are required for the whole reaction channel and the propagation of wave packet in a 9-D PES is very challenging. It is also not easy to construct the Hamiltonian and wave function for wave packet propagation in full dimension. In this context the role of approximate methods which would not level down the accuracy of results but reduce the computational effort are highly acknowledged[42,43]. One such method is Reaction Path Hamiltonian (RPH) for polyatomic molecules, based on the RPH method proposed by Miller *et al.*[44] and developed by Jackson and co-workers[27,45]. In this method we need to construct a single-dimensional reaction path, as the reaction path is an abstract one-dimensional path connecting the minima and the saddle point. As a result a much less number of *ab initio* data points are required. It also include the tunneling process. Jackson *et al*. have reported studies of dissociative chemisorption of methane on Ni and Pt surfaces using the RPH formulation and successfully explained the dynamical behavior of the reaction[45,46]. The same group have also performed quantum dynamics calculations of H_2O, HOD and D_2O dissociation on closed-packed Ni(111) surface[32]. In summary RPH have been used and is capable of reproducing and validating experimental trends in reactivity comprising of mode and bond selectivity.

The aim of this work is to study the rate determining step of water-gas-shift reaction, i.e. dissociation of water on Ni(211) step surface. The rationale behind the choice of using step surface is due to its increasing attention recently as it lowers activation energy barrier for all surface reaction than that of at (111) surfaces. Our main objective here is to understand the dynamical behavior and mode-selectivity and how it differs from (111) flat surface. We study the effect of lattice motion coupled with semi-classical method, that in turn include the effect of surface temperature in detail. That help us to understand the effect of surface temperature on reactivity. We also try to understand the effect of excitation of different vibrational modes of water in adiabatic potential energy surface i.e. which mode is more reactive for the dissociation process under the approximation of vibrational adiabaticity. In Section 2. a brief review of RPH model is given along with semi-classical tunneling formulation and computational method. In Section 3. we present our result for the effect of surface temperature on reactivity and reaction probability of water molecule on Ni(211) surface. In Section 4, we summarize our result.

2. Methodology

Density functional theory calculations

All total energy calculations were performed by using DFT based Vienna *ab-initio* simulation package (VASP)[47–50]. Non local exchange-correlation effects are treated using plane wave basis set and Perdew-Burke-Ernzerhof (PBE)[51,52] exchange-correlation functional within generalized gradient approximation (GGA). Fully non local optimized projector augmented wave (PAW)[53,54] potentials are used to express the interaction between the ionic cores and electrons. As there is a magnetic element of Ni is involved in the system the spin polarized calculations have been performed with the plane wave expansion truncated at 400 eV. Metal surfaces were modeled as asymmetric slab supercell model with periodic boundary conditions. Ni(211) surfaces consist of four layers within 3×1 unit cell. Ni(211) surface is consist of three atom wide (111) terrace and one atom high (100) steps as shown in Fig. 1. A large vacuum space have been used along z axis

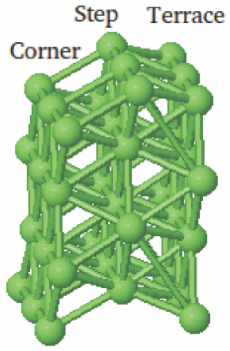

Fig. 1. A model representation of three layer supercell for Ni(211), indicating three different surface atoms: step, terrace and corner.

(approx. 18 Å) to avoid any interaction between a surface and its repeated image along the z-direction. Equilibrium lattice constants for Ni is 3.52 Å found from the bulk geometry optimization in VASP are used for all the calculations. 8×8×1 Γ centred grid of *k*-points were used for structure optimization. All the atoms were allowed to relax during structure optimization of Ni(211) surface. During adsorption calculations only adsorbate molecules were kept relaxed and the metal surface kept fixed. All the calculations are considered to be converged when the forces on all atoms are smaller than 0.01 eV/Å. Climbing image nudged elastic band (CI-NEB) method[55] has been used for identifying the transition state geometries, for which the converging criteria is when all the forces are less than 0.05 eV/Å. The transition state was verified by frequency calculation, confirming a negative frequency is there. Adsorption energy was calculated using the expression, $E_{ads} = E_{(adsorbate+surface)} - [E_{adsorbate} + E_{surface}]$, where E_{ads}, $E_{(adsorbate+surface)}$, $E_{adsorbate}$ and $E_{surface}$ are the adsorption energy, energies of the adsorbed systems, molecule in the gas phase and metal slab respectively.

Lattice motion

During calculations of adsorption energies of H, OH or H_2O and reaction paths all the metals atoms were kept frozen. However, inclusion of motion of lattice atom has been shown to change the activation energy barrier and increase reaction probability with increasing surface temperature[56]. To include the effect of lattice motion a simple, successful and physically meaningful model known as 'sudden model'[57–59] is used. In this model, two linear coupling parameters β (electronic coupling), α (mechanical coupling) which are dened by $\Delta E_{barrier} = -\beta\Delta Q$ and $\Delta Z_{barrier} = \alpha\Delta Q$ are calculated. Here, $\Delta E_{barrier}$ and $\Delta Z_{barrier}$ are defined as change in barrier height and change in location of transition state, respectively, with change of position of lattice atom, over which H_2O molecule adsorbed, from its equilibrium position (Q = 0). Q is the lattice degree of freedom perpendicular to surface which is chosen to vary a maximum of 0.2 Å both upwards and downwards from its equilibrium position (Q = 0). Further details of the sudden model can found elsewhere[60,61].

The lattice atom of the surface over which water molecule get adsorbed, force on that atom is significant in the transition state compared to other metal atoms on the surface. In other word the transition state is modified to a good approximation by the motion of the atom over which water molecule is adsorbed. The minimum energy path is described by a mass-weighted coordinate s, with nine degrees of freedom for a fixed value of Q. The potential energy surface is approximated as an inverted parabola, with width equal to $|i\omega_9(0)|^2$, where $\omega_9(0)$ is the imaginary frequency in the transition state. The semi-classical tunneling probability is given by

$$P(E;Q) = \frac{1}{1+e^{b(E_b-\beta Q-E)}} \approx e^{b(E-E_b+\beta Q)} \qquad (1)$$

where, b is given as $\frac{2\pi}{\hbar|\omega_9(0)|}$. $P(E;Q)$ is the dissociation probability at a given incident energy E and lattice degree of freedom Q. By doing Boltzman average over all possible values of Q, dissociation probability is calculated at different surface temperature. The temperature dependent reaction probability is given by

$$P_r(E;T) = \int_{-\infty}^{\infty} e^{b(E-E_b+\beta Q)} \sqrt{\frac{M\Omega^2}{2\pi kT}} \exp\left(-\frac{M\Omega^2 Q^2}{2kT}\right) dQ \qquad (2)$$

Here metal atom of mass M moves harmonically with a frequency Ω for a given incident energy E, at a given surface temperature T. Reaction probability, calculated this way is dependent only on the electronic coupling parameter β. Further inclusion of mechanical coupling parameter, α i.e. and by averaging over lattice atom momentum P, dissociation probability improved.

$$S(E;T) = \int dE_{cm} \sqrt{\frac{M'_s}{4\pi kT\mu_T E_{cm}}} \exp\left[-\frac{M'_s}{2kT} \left(\sqrt{\frac{2E_{cm}}{\mu_T}} - \sqrt{\frac{2E}{M}} \right)^2 \right] P_r(E;T) \quad (3)$$

Here, E_{cm} stands for center-of-mass energy of the incoming molecule and Z and Q coordinates are transformed to a relative coordinate $Z' = Z - \alpha Q$ and a corresponding center-of-mass coordinate[62], thus reduced mass corresponding to the relative collision coordinate Z' is $\mu_T = \frac{M'_s M}{(M'_s + M)}$, where $M'_s = \frac{M_s}{\alpha^2}$.

Theory of RPH

Hamiltonian for dissociation of any molecule over a rigid metal lattice is given by

$$H = K + V = -\frac{\hbar^2}{2} \sum_{i=1}^{9} \frac{\partial^2}{\partial x_i^2} + V(x_1, x_2, \ldots, x_9) \quad (4)$$

where x_i are the nine mass-weighted Cartesian coordinate for H_2O nuclei. We first locate the minimum energy path from the transition state to the reactant and product to form the PES, V. Along this reaction path several images (molecular configurations) was located. These images were optimised using CI-NEB method[55]. The distance between these images along the reaction path is given by s, reaction path coordinate. Where $(ds)^2 = \sum_{i=1}^{9} (dx_i)^2$ and at the transition state $s = 0$, and positive and negative s values corresponds to product and reactant side respectively. The 1-D PES is constructed by calculating the total energy $V_0(s)$ along this reaction path at various images. To find 8 normal mode vibrational coordinates Q_k and corresponding frequencies $\omega_k(s)$, diagonalization of Hessian was performed. Eigenvector $L_{i,k}$ describing motion orthogonal to reaction path. Within the harmonic approximation the PES in the reaction path coordinate s and Q_k is given by,

$$V = V_0(s) + \sum_{k=1}^{8} \frac{1}{2} \omega_k^2(s) Q_k^2(s) \quad (5)$$

Relation between 9 mass-weighted coordinate x_i and normal mode coordinate Q_k with respect to s is given by

$$x_i = a_i(s) + \sum_{k=1}^{8} L_{i,k}(s) Q_k \,, \quad (6)$$

here $a_i(s)$ describes the conguration of the molecule at point s. In the reaction path coordinate, the Hamiltonian of eq. (1) is written as[44]

$$H = p_s^2 + V_0(s) + H_{vib} - \frac{1}{4} (b_{ss} p_s^2 + 2 p_s b_{ss} p_s + p_s^2 b_{ss}) - \frac{1}{2} (p_s \pi_s + \pi_s p_s) \quad (7)$$

where

$$H_{vib} = \sum_{k=1}^{8} \left[\frac{1}{2} P_k^2 + \frac{1}{2} \omega_k^2(s) Q_k^2 \right] \quad (8)$$

p_s and p_k are momenta conjugate to s and Q_k, respectively, and

$$b_{ss} = \sum_{k=1}^{8} Q_k B_{k,9}(s), \; \pi_s = \sum_{k=1}^{8} \sum_{j=1}^{8} Q_k P_j B_{k,j}(s) \quad (9)$$

The vibrationally non-adiabatic coupling $B_{k,j}(s)$, is defined as

$$B_{k,j}(s) = \sum_{k=1}^{8} \frac{dL_{l,k}}{ds} L_{i,j}(s) \quad (10)$$

Hamiltonian in eq. (7) is expanded upto first order, as higher order terms are not so important[63,64]. Energy flow between two different modes k and j through coupling $B_{k,j}$ is described by the operator π_s and the coupling between a vibrational mode with the reaction coordinate is given by coupling $B_{k,9}$ that is described by operator b_{ss}.

The close-coupled wave packet approach is used to describe the total molecular wave function, that is written as:

$$\Psi(s;t) = \sum_n \chi_n(s;t) \Phi_n \left(\{Q_k\} \right) s \quad (11)$$

where Φ_n are the eigenfunction of H_{vib}, with eigenvalues $\sum_{k=1}^{8} \hbar\omega_k(s) \left(n_k + \frac{1}{2} \right)$, where index n in eq. (11) corresponds to the set of quantum numbers $\{n_k\}$. These vibrationally adiabatic eigenfunctions are product of 1-D harmonic oscillator that depends parametrically on s. The molecular wave function $\Psi(t)$ and the Hamiltonian of eq. (7), coupled equation of motion for the wave packets, $\chi_n(s;t)$ are

of the form

$$i\hbar\frac{\partial\chi_n(s;t)}{\partial t} = \left[\frac{1}{2}{p_s}^2 + V_0(s) + \sum_{k=1}^{8}\hbar\omega_k(s)\left(n_k+\frac{1}{2}\right)\right]$$
$$\chi_n(s;t) + \sum_{n'}F_{nn'}\chi_{n'}(s;t) \quad (12)$$

These wave packets thus evolve on vibrationally adiabatic potential energy surfaces for each vibrational state n. This vibrationally adiabatic potential over which the wavepackets propagate, is given by

$$V_{\text{eff},n}(s) = V_0(s) + \sum_{k=1}^{8}\hbar\omega_k(s)\left(n_k+\frac{1}{2}\right) \quad (13)$$

These effective potentials are zero point energy corrected MEP and the energy of any vibrational excitation, that can change along the path. The operators $F_{nn'}$ contain coupling operator b_{ss} and π_s that couple one and two quanta excited vibrationally adiabatic states, respectively. The parametric dependence of Φ_n on s results in derivative coupling terms that are responsible for curve crossing at higher velocities and for large coupling values[45,46,65]. Among nine modes of water, six is included with highest frequencies near the transition state in the vibrationally adiabatic basis set. The other two modes have almost zero frequency in the whole reaction path and corresponds to the azimuthal orientation of the reacting O-H bond in the plane of surface. Energy varies weakly with these type of motions. Standard techniques[45,46] are used to propagate the wave packets in time, and the reactive flux at large s is Fourier transformed in time at each channel to give vibrationally state resolved and energy resolved reaction probabilities[66,67]. This is denoted as static surface reaction probability $P_0(E_i,n)$. The change of position of H_2O molecule in the X and Y direction is small along the MEP in the entrance channel and upto the TS. Due to the very low frequency rotational motion is treated adiabatically and do not coupled to other modes.

3. Results and discussion

Adsorption energy, E_{ads} was computed for a hydrogen atom and OH at different high symmetry binding sites on Ni(211) surface. H atom gets strongly bound on the HCP hollow site between step edge and terrace atoms, with adsorption energy –2.80 eV and on the step edge bridge site with adsorption energy –2.72 eV. Along the (111) terrace atom bridge site adsorption energy of hydrogen is –2.74 eV. In the lower step hollow site adsorption energy is –2.78 eV.

For OH adsorption, binding energy variation is much larger depending on the adsorbing site. Strongly bound adsorption site for OH is on the step-edge bridge site with adsorption energy –3.40 eV, where the distance of 'O' from two step site Ni atoms is 1.91 Å. In this case the H atom of OH pointing towards the lower step site. In the scenario when H atom point towards the upper step the adsorption energy is almost same, –3.38 eV. Distance between O atom of OH and step site Ni atom is 1.92 Å. On the other hand OH adsorption energy on the (111) terrace site is much lower, –2.79 eV. In this case distance of 'O' and terrace Ni atoms is 2 Å. OH molecule does not prefer any hollow site for its adsorption.

As mentioned above all the TS calculations were performed using CI-NEB method. In the transition state calculation water molecule on the top site of a step Ni atom is treated as initial state. Here distance between water molecule and step Ni atom is 2.14 Å and water molecule is physisorbed here. H and OH coadsorbed state is treated as the final state. In the coadsorption process when both H and OH are placed on their most stable sites individually, i.e. OH on the bri-edge site and H is on the HCP hollow site between step edge and terrace atoms there is a strong repulsion between OH and H. In that case coadsorption energy is –5.54 eV. On the other hand when coadsorption is performed with OH in its most stable site and H is on the bridge site of (111) terrace atom, that leads to most stable coadsorption site. This coadsorption energy is –6.65 eV. We use this coadsorption site as the final state for NEB calculation. In Figs. 2 and 3 we have shown the side and top view respectively of initial, transition and final state of water dissociation on a Ni(211) surface. Activation energy barrier is found to be 0.84 eV, which is much higher compared to previous report of water dissociation on Ni(211) step surface (0.51 eV)[68]. This might be due to different reasons. In the reference of Wang *et al.* work[68], they have used 3×2 and 3×4 supercell and in this work dimension of supercell is 3×1. Using smaller supercell sometimes leads

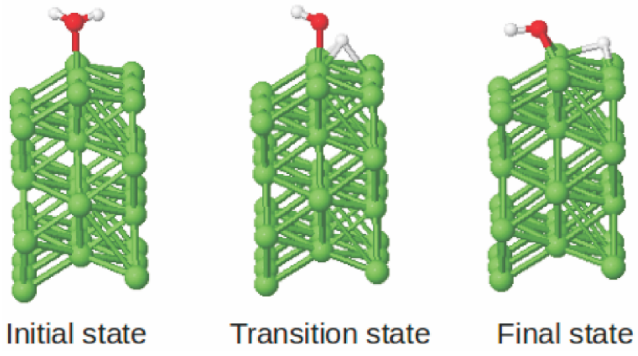

Fig. 2. Side view of initial, transition and final state of water dissociation on a Ni(211) surface

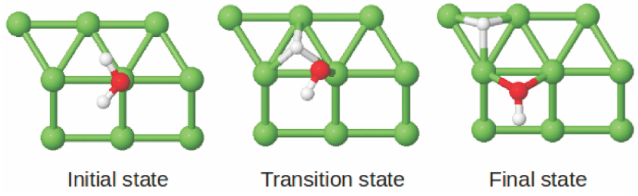

Fig. 3. Top view for initial, transition and final state of water dissociation on a Ni(211) surface.

to higher activation energy barrier[69]. This might be due to the fact that in case of smaller supercell two fragments of water dissociation products i.e. H and OH are much closer to one another which leads to destabilization of the product. In case of larger supercell we have large space on the supercell to accommodate two product fragments, hence lesser repulsion between them and no destabilization of the product as that of smaller supercell. The final state that we use in the calculation is most stable state. Although using most stable final state does not guarantee to obtain lowest activation energy barrier for the dissociation process[70]. Activation energy barrier also depends on the initial state geometry, i.e. adsorption of H_2O on the step surface, for H_2O dissociation process. Water molecule can be adsorbed with different orientation on a step surface, that leads to different adsorption energy. Therefore one should carry out the transition state calculation for all possible initial as well as final states for a given supercell. However, our main objective in this work is to find out the effect of surface temperature on reactivity and to study the dynamics of reaction. To understand the effect of surface temperature on reactivity first we calculate the the electronic and mechanical coupling parameters, α and β respectively, as mentioned in the Lattice Motion part under Methodology at Section 2. For that we calculate the activation energy barrier for four different Q (lattice atom coordinate) values apart from $Q = 0$, i.e. equilibrium position of surface lattice atom according to prescription given in theory. Table 1 enlists all the transition states data for water dissociation on Ni(211) surface for all five lattice atom coordinates. Meaning of each parameter is provided in the caption of the Table 1 above.

Table 1. Table for different transition state data for water dissociation on Ni(211) surface. Q represents coordinate of lattice atom on which water molecule adsorbed. E_a is the activation energy barrier. $r_{O\text{-}H}$ is the distance of dissociating O-H bond. Θ_{HOH} is angle between H and OH and Z is the distances of H_2O molecule from step surface

Q(Å)	E_a (eV)	$r_{O\text{-}H}$ (Å)	Θ_{HOH} (°)	Z (Å)
+0.2	0.73	1.55	128.75	1.82
+0.1	0.80	1.51	132.89	1.85
0	0.84	1.49	134.00	1.87
–0.1	0.88	1.44	132.92	1.91
–0.2	0.91	1.42	129.44	1.93

To get the value of coupling parameters β and α we plot E_a (eV) and Z (Å) against Q (Å), respectively and t them linearly. These two plots are given in Fig. 4.

From the fitted plot we obtain β and α values as 0.44 eV/Å and 0.28, respectively. This β coupling parameter, i.e. coupling parameter is nothing but the force experienced by the step lattice metal atom when water molecule is approaching towards it. This β value matches exactly that we get from our DFT calculation. After obtaining the value of β, using eq. (2) reaction probability was calculated using semi-classical model for four different surface temperatures, 0 K, 100 K, 300 K and 500 K. This reaction probability is plotted in Fig. 5. As suggested this reaction probability is further improved by the inclusion of mechanical coupling parameter, α. Reaction probability plot including α is shown in Fig. 6. For more clear understanding of effect of inclusion of β and α, in Fig. 7 the reaction probability is shown for three different cases. (i) For both α and β is zero, i.e. rigid lattice condition, where there is no molecule phonon coupling. (ii) Include only electrical coupling parameter (β). (iii) Include both electronic and mechanical coupling parameter. Inclusion of α coupling de-

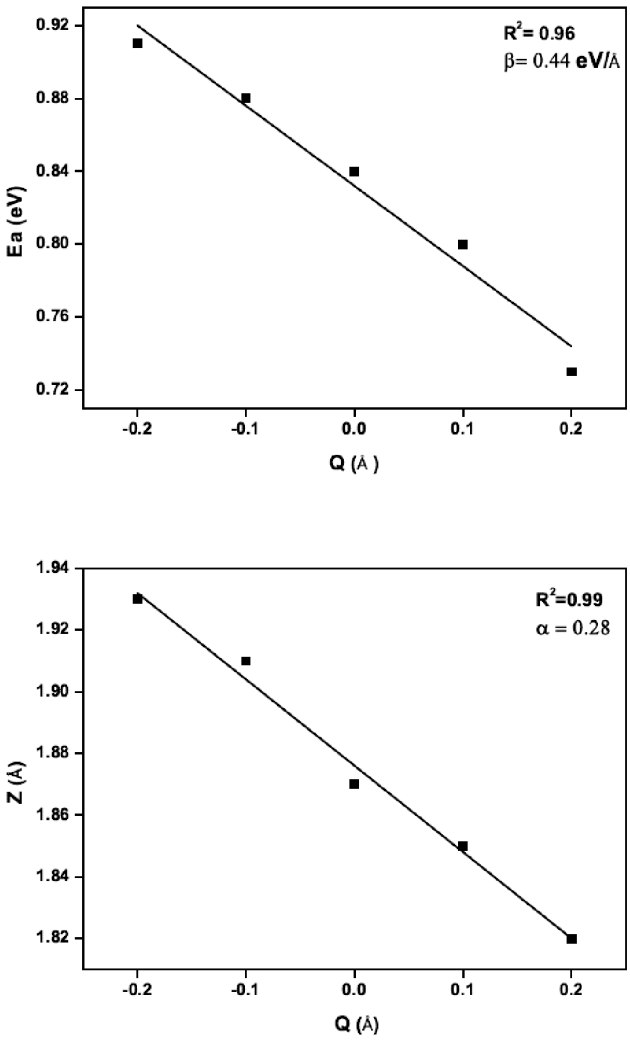

Fig. 4. Plot of E_a vs Q and Z vs Q for α and β values. Upper plot is the plot of E_a vs Q and lower plot is for Z vs Q. These two plots are done by taking data from Table 1.

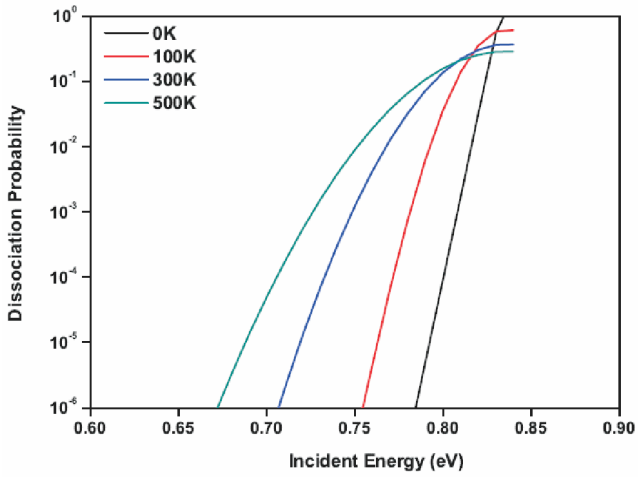

Fig. 5. Plot of dissociation probability vs incident energy by including only β coupling parameter using semi-classical tunneling model.

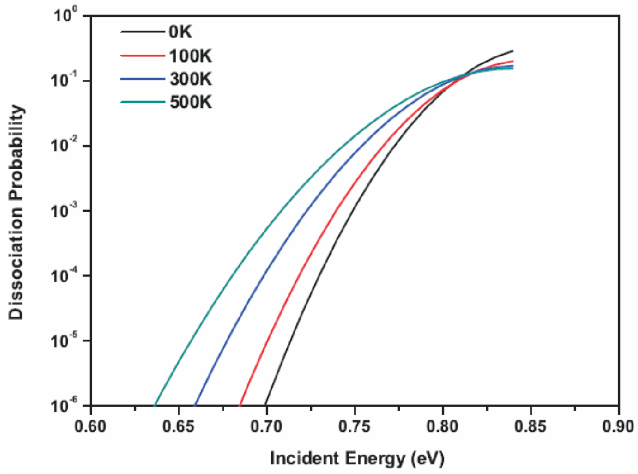

Fig. 6. Plot of dissociation probability vs incident energy by include both β and α coupling parameters using semi-classical model.

crease the reaction probability at high energy, due to lattice recoil effect. Whereas reaction probability increase at low incident energy due to larger relative collision velocity[71–73].

To look how the different normal modes of H_2O behave during reaction in Fig. 8a and 8b, we plot frequencies of different normal modes of water molecule along the reaction path. In Fig. 8a, all the normal modes of H_2O molecule has shown except the symmetric stretching mode whereas in Fig. 8b only symmetric stretching mode has shown. When water molecule is far above the surface that means at large negative s value, frequency of three normal modes, i.e. asymmetric stretching (ν_{as}), symmetric stretching (ν_{ss}) and bending (ν_b) modes are non-zero. These are asymptotically bound modes. Other five modes corresponds to rotational and translational motion. Frequency of these modes are nearly zero when water molecule is far away from the surface. These are asymptotically unbound states. Frequency of asymmetric stretching mode remains unchanged throughout the whole reaction path. Frequency of symmetric stretching and bending modes, on the other hand, decrease significantly near the transition state. Other five rotational and translational modes become frustrated near the transition state and thus

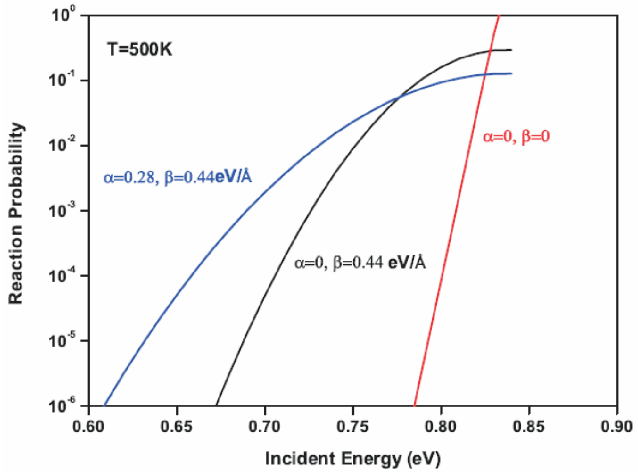

Fig. 7. Plot of dissociation probability vs incident energy for comparison of α and β coupling parameters individually.

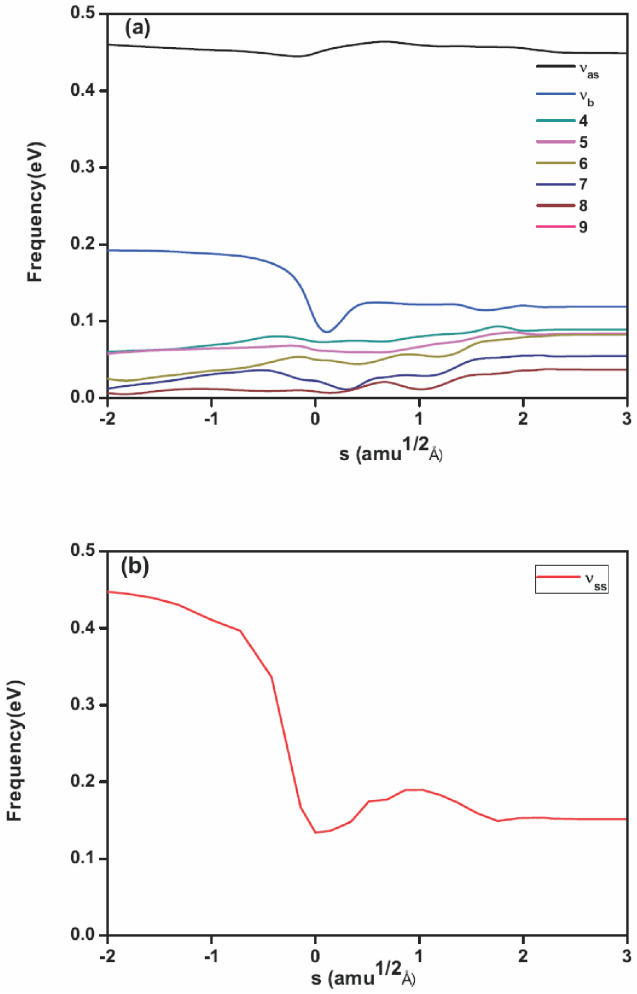

Fig. 8. Frequencies of different normal modes of water along the reaction path for water dissociation on Ni(211) surface. ν_{as} corresponds to asymmetric stretching mode, ν_{ss} corresponds to symmetric stretching mode and ν_b corresponds to bending mode. Other numbered modes are representing frustrated translation and rotation modes. In (a) panel all other vibrational modes are showing except the symmetric stretching mode and in panel (b) variation of only symmetric stretching mode along the reaction path has shown.

no much change of frequency is observed. We are concerned over the vibrational mode selectivity, so low frequency modes are not so important here. Softening of the symmetric stretching and bending mode suggests that excitation of this two modes would lead to higher reaction probability under adiabatic approximation. Excitation of asymmetric mode would not lead to enhancement of reaction probability significantly. This statement could be understood better from Fig. 9, where we plot ZPE corrected barrier height and barrier height for one-quantum excitation of diffierent vibrational normal modes of water. It can be seen from the plot that inclusion of ZPE correction lowers the barrier height significantly. For ground state it lowers the barrier height by 0.18 eV. It is evident from this plot that symmetric stretching mode barrier height is the lowest, as predicted from frequency calculation followed by bending and asymmetric mode. Static surface reaction probability for H_2O dissociation on Ni(211) surface is calculated for adiabatic case and plotted in Fig. 10. Within the vibrationally adiabatic limit, ground vibrational state shows lowest reaction probability. Among the normal vibrational modes, symmetric stretching mode shows the highest reaction probability. Asymmetric mode shows slightly higher reaction probability than the ground state. In case of bending mode, the reaction probability values are in between symmetric and asymmetric stretching mode. These behaviors of reaction probability within the vibrational adiabatic limit can be explained by significant decrease of effective barrier height of different normal modes with respect to ground state (Fig. 9). This observation can be correlated with the fact that there is a significant mode softening was observed for symmetric stretch and bending mode. Asymmetric stretching mode on the other hand does not exhibit significant mode softening. Therefore within vibrational adiabatic approximation the order of reaction probability is : $V_{ss} > V_b > V_{as} > V_{zpc}$.

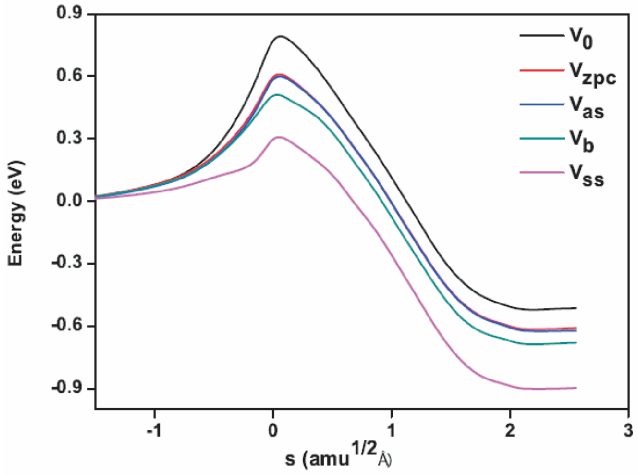

Fig. 9. Vibrational zero point energy (ZPE) corrected potential for ground vibrational state and potential corresponds to one quantum excitation of symmetric, asymmetric and bending modes of H_2O. V_{zpc} is ZPE corrected ground state potential and V_{ss}, V_{as} and V_b corresponds to ZPE corrected symmetric, asymmetric and bending modes of H_2O.

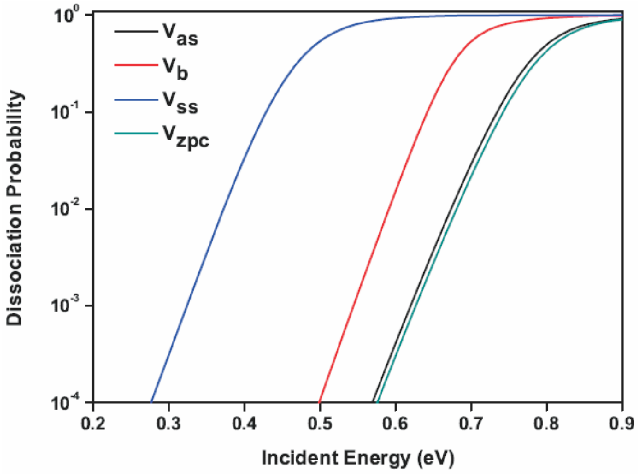

Fig. 10. Adiabatic reaction probabilities for different vibrational normal modes and ground state vibration of H_2O molecule under rigid lattice approximation. Meaning of V_{zpc}, V_{ss}, V_{as} and V_b has given in the caption of Fig. 8.

4. Conclusions

Water dissociation process has been studied on a step surface Ni(211). It has been observed that when water molecule is approaching towards the surface of the catalyst, the atom over which water molecule is adsorbed, feels a force and puckered outwards. In other words molecule-phonon coupling is significant during dissociation process. Surface temperature effect was included in the calculation by taking account of the molecule-phonon coupling parameters, β and α, electronic and mechanical coupling parameters respectively. It has been found that with increase of surface temperature reaction probability increases significantly. Effect of both coupling parameters, β and α has been shown individually.

Dynamics study of this dissociation process was also performed using Reaction Path Hamiltonian method. Minimum energy path was determined and the normal mode analysis was performed on all the points along the minimum energy path. From this normal mode analysis it was found that frequency of symmetric stretching mode decrease significantly near the TS and also that of bending mode. But asymmetric mode remain constant in the whole channel. Due to this mode softening of symmetric and bending mode when molecule enters the TS, has an effect on activation energy barrier. It decreases the energy barrier significantly with respect to ground state, as a result of that reaction probability is highest for the symmetric stretching mode and second highest for the bending mode, which shows somewhat less mode softening in the normal mode analysis. Asymmetric and ground state reaction probability on the other hand are nearly similar and show low reaction probability, compared to that of symmetric stretching and bending modes.

However, one should perform the full coupling calculation i.e. taking into account the vibrational non-adiabaticity. This will allow the energy flow between different modes of vibration as well as flow of energy between the reaction path and the individual normal modes. All the reaction probability calculation that has been performed in this work is under rigid lattice approximation. But we have already mentioned that molecule-phonon coupling is significant in this type of processes. Therefore, it is also necessary to include electronic and mechanical coupling parameter during the dynamics calculation of the reaction, which in turn will also include temperature effect on the reaction probability using the same RPH formulation. This calculations are under progress and will be published subsequently somewhere else.

Acknowledgement

SR thanks CSIR, India for fellowship under Grant No. 09/921(0126)/2015-EMR-I. NKJ thanks Inspire scholarship, India for her fellowship. AKT thanks SERB, New Delhi, India for funding through Project No. EMR/2015/001337.

References

1. C. Ratnasamy and J. P. Wagner, *Catalysis Reviews*, 2009, **51**, 325.
2. M. A. Henderson, *Surf. Sci. Rep.*, 2002, **46**, 1.
3. P. A. Thiel and T. E. Madey, *Surf. Sci. Rep.*, 1987, **7**, 211.
4. G. Busca, U. Costantino, F. Marmottini, T. Montanari, P. Patrono, F. Pinzari and G. Ramis, *Appl. Catal. A*, 2006, **310**, 70.
5. N. Schumacher, A. Boisen, S. Dahl, A. A. Gokhale, S. Kandoi, L. C. Grabow, J. A. Dumesic, M. Mavrikakis and I. Chorkendor, *J. Catal.*, 2005, **229**, 265.
6. A. A. Gokhale, J. A. Dumesic and M. Mavrikakis, *J. Am. Chem. Soc.*, 2008, **130**, 1402.
7. C. Ovensen and P. Stoltze, *J. Catal.*, 1992, **134**, 445.
8. C. A. Callaghan, S. A. Vilekar, I. Fishtik and R. Datta, *Appl. Catal. A*, 2008, **345**, 213.
9. S. Ghosh, S. Hariharan and A. K. Tiwari, *J. Phys. Chem. C*, 2017, **121**, 16351.
10. A. A. Phatak, W. N. Delgass, F. H Ribeiro and W. F. Schneider, *J. Phys. Chem. C*, 2009, **113**, 7269.
11. J. L. C. Fajín, D. S. Cordeiro, M. N. and J. R. B. Gomes, *J. Phys. Chem. A*, 2014, **118**, 5832.
12. S. C. Huang, C. H. Lin and J. H. Wang, *J. Phys. Chem. C*, 2010, **114**, 9826.
13. D. Sebastiani and L. Delle Site, *J. Chem. Theory. Comput.*, 2005, **1**, 78.
14. A. Mondal, H. Seenivasan and A. K. Tiwari, *J. Chem. Phys.*, 2012, **137**, 094708.
15. B. Jiang, J. Li, D. Xie and H. Guo, *J. Chem. Phys.*, 2013, **138**, 044704.
16. B. Jiang and H. Guo, *Phys. Rev. Lett.*, 2015, **114**, 166101.
17. D. Ray, S. Ghosh and A. K. Tiwari, *J. Phys. Chem. A*, 2018, **122**, 5698.
18. A. Farjamnia and B. Jackson, *J. Chem. Phys.*, 2015, **142**, 234705.
19. S. Ghosh, D. Ray and A. K. Tiwari, *J. Chem. Phys.*, 2019, **150**, 114702.
20. H. Seenivasan, B. Jackson and A. K. Tiwari, *J. Chem. Phys.*, 2017, **146**, 074705.
21. F. F. Crim, *Science*, 1990, **249**, 1387.
22. F. F. Crim, *Acc. Chem. Res.*, 1999, **32**, 877.
23. D. R. Killelea, V. L. Campbell, N. S. Shuman and A. L. Utz, *Science*, 2008, **319**, 790.
24. L. Chen, H. Ueta, R. Bisson and R. D. Beck, *Faraday Discuss.*, 2012, **157**, 285.
25. R. D. Beck, P. Maroni, D. C. Papageorgopoulos, T. T. Dang, M. P. Schmid and T. R. Rizzo, *Science*, 2003, **302**, 98.
26. R. Smith, D. Killelea, D. DelSesto and A. Utz, *Science*, 2004, **304**, 992.
27. S. Nave, A. K. Tiwari and B. Jackson, *J. Phys. Chem. A*, 2014, **118**, 9615.
28. P. M. Hundt, H. Ueta, M. E. van Reijzen, B. Jiang, H. Guo and R. D. Beck, *J. Phys. Chem. A*, 2015, **119**, 12442.
29. B. Jiang, X. Ren, D. Xie and H. Guo, *Proc. Natl. Acad. Sci.*, 2012, **109**, 10224.
30. B. Jiang, D. Xie and H. Guo, *Chem. Sci.*, 2013, **4**, 503.
31. P. M. Hundt, B. Jiang, M. E. van Reijzen, H. Guo and R. D. Beck, *Science*, 2014, **344**, 504.
32. A. Farjamnia and B. Jackson, *J. Chem. Phys.*, 2015, **142**, 234705.
33. H. Seenivasan and A. K. Tiwari, *J. Chem. Phys.*, 2013, **139**, 174707.
34. B. Jiang and H. Guo, *J. Chem. Phys.*, 2015, **143**, 164705.
35. A. T. Gee, B. E. Hayden, C. Mormiche, A. W. Kleyn and B. Riedmnuller, *J. Chem. Phys.*, 2003, **118**, 3334.
36. F. Abild-Pedersen, O. Lytken, J. Engbk, G. Nielsen, I. Chorkendor and J. K. Nørskov, *Surf. Sci.*, 2005, **590**, 127.
37. B. Jiang, *Chem. Sci.*, 2017, **8**, 6662.
38. T. Liu, Z. Zhang, B. Fu, X. Yang and D. H. Zhang, *Phys. Chem. Chem. Phys.*, 2016, **18**, 8537.
39. P. M. Hundt, B. Jiang, M. E. van Reijzen, H. Guo and R. D. Beck, *Science*, 2014, **344**, 504.
40. T. Liu, B. Fu and D. H. Zhang, *Phys. Chem. Chem. Phys.*, 2017, **19**, 11960.
41. E. D. German and M. Sheintuch, *J. Phys. Chem. C*, 2010, **114**, 3089.
42. H. Guo, *Theor. Chem. Acc.*, 2012, **131**, 1077.
43. K. Golibrzuch, N. Bartels, D. J. Auerbach and A. M. Wodtke, *Annu. Rev. Phys. Chem.*, 2015, **66**, 399.
44. W. H. Miller, N. C. Handy and J. E. Adams, *J. Chem. Phys.*, 1980, **72**, 99.
45. B. Jackson and S. Nave, *J. Chem. Phys.*, 2011, **135**, 114701.
46. B. Jackson and S. Nave, *J. Chem. Phys.*, 2013, **138**, 174705.
47. G. Kresse and J. Hafner, *Phys. Rev. B*, 1993, **47**, 558.
48. G. Kresse and J. Hafner, *Phys. Rev. B*, 1994, **49**, 14251.
49. G. Kresse and J. Furthmnuller, *Comput. Mater. Sci.*, 1996, **6**, 15.
50. G. Kresse and J. Furthmnuller, *Phys. Rev. B*, 1996, **54**, 11169.
51. J. P. Perdew, K. Burke and M. Ernzerhof, *Phys. Rev. Lett.*, 1996, **77**, 3685.

52. J. P. Perdew, K. Burke and M. Ernzerhof, *Phys. Rev. Lett.*, 1997, **78**, 1396.
53. P. E. Blnochl, *Phys. Rev. B*, 1994, **50**, 17953.
54. G. Kresse and D. Joubert, *Phys. Rev. B*, 1999, **59**, 1758.
55. G. Henkelman, B. P. Uberuaga and H. Jónsson, *J. Chem. Phys.*, 2000, **113**, 9901.
56. H. Guo, A. Farjamnia and B. Jackson, *J. Phys. Chem. Lett.*, 2016, **7**, 4576.
57. A. K. Tiwari, S. Nave and B. Jackson, *Phys. Rev. Lett.*, 2009, **103**, 253201.
58. A. K. Tiwari, S. Nave and B. Jackson, *J. Chem. Phys.*, 2010, **132**, 134702.
59. S. Nave, A. K. Tiwari and B. Jackson, *J. Chem. Phys.*, 2010, **132**, 054705.
60. B. Jackson. in: 'Dynamics of Gas-Surface Interactions: Atomic-level Understanding of Scattering Processes at Surfaces', eds. R. Díez Muiño and H. F. Busnengo, Springer, Berlin, Heidelberg, 2013, pp. 213-237.
61. S. Nave, A. K. Tiwari and B. Jackson, *J. Phys. Chem. A*, 2014, **118**, 9615.
62. A. C. Luntz and J. Harris, *Surf. Sci.*, 1991, **258**, 397.
63. M. Mastromatteo and B. Jackson, *J. Chem. Phys.*, 2013, **139**, 194701.
64. B. Jackson, F. Nattino and G.-J. Kroes, *J. Chem. Phys.*, 2014, **141**, 054102.
65. S. Nave and B. Jackson, *Phys. Rev. B*, 2010, **81**, 233408.
66. D. Zhang, Q. Wu and J. Z. H. Zhang, *J. Chem. Phys.*, 1995, **102**, 124.
67. J. Dai and J. Z. H. Zhang, *J. Chem. Phys.*, 1996, **100**, 6898.
68. Y. Huang, C. Ling, M. Jin, J. Du, T. Zhou and S. Wang, *Phys. Chem. Chem. Phys.*, 2013, **15**, 17804.
69. H. Guo, J. P. Menzel and B. Jackson, *J. Chem. Phys.*, 2018, **149**, 244704.
70. S. Nave and B. Jackson, *J. Chem. Phys.*, 2009, **130**, 054701.
71. J. Harris, J. Simon, A. C. Luntz, C. B. Mullins and C. T. Rettner, *Phys. Rev. Lett.*, 1991, **67**, 652.
72. A. Luntz and J. Harris, *Surf. Sci.*, 1991, **258**, 397.
73. M. Hand and J. Harris, *J. Chem. Phys.*, 1990, **92**, 7610.